Available online at www.sciencedirect.com
ScienceDirect
Polymer 48 (2007) 4242–4251
polymer
www.elsevier.com/locate/polymer

Fibrillation of liquid crystalline polymer in polysulfone promoted by increased system elasticity via adding nano-silica

Jun Chen [a,b], Peng Chen [a,b], Lichuan Wu [a,b], Jun Zhang [a], Jiasong He [a,*]

[a] *Beijing National Laboratory for Molecular Sciences (BNLMS), Key Laboratory of Engineering Plastics, Joint Laboratory of Polymer Science and Materials, Institute of Chemistry, Chinese Academy of Sciences, Beijing 100080, China*
[b] *Graduate School, Chinese Academy of Sciences, Beijing 100039, China*

Received 19 January 2007; received in revised form 23 April 2007; accepted 7 May 2007
Available online 13 May 2007

Abstract

Ternary blends composed of a liquid crystalline polymer (LCP), nano-SiO_2 and polysulfone (PSF) were prepared by melt blending. Very long and perfectly oriented LCP fibrils were in situ formed in capillary flows by adding 5 vol% of nano-SiO_2 to binary PSF/LCP blend. Dynamic rheology analysis indicated that the sharp increase of elasticity was caused by higher content of nano-SiO_2. Then the entrance angle was decreased and elongational stress increased when the polymer melt flowed through the abrupt contraction, which resulted in the fibrillation of LCP in PSF/LCP/nano-SiO_2 system.
© 2007 Elsevier Ltd. All rights reserved.

Keywords: Polysulfone; Liquid crystalline polymers (LCP); Nano-SiO_2

1. Introduction

Polymer blending is a useful and attractive approach to new polymeric materials with more balanced properties than their components. Most polymers are immiscible so that during the processing these component polymers form a multi-phase system in their blends with a variety of morphology of the dispersed phase such as droplets, fibrils, lamellae, and co-continuous structure. Since the morphology of polyblends affects the multiplicity of physical and mechanical properties, it is of great importance to know the formation of these complicated morphologies and their control during material processing. Several factors such as the composition, viscosity ratio, elasticity ratio, interfacial tension, shear rate and mixing time have their own influences on the final morphology of the phases. Up to now many good results showing the relationship between morphology and respective factors have been obtained [1–8].

Based on the knowledge of blending flexible chain polymers, blending semi-rigid chain polymers with flexible chain polymers has been widely investigated by many researchers. Termed as in situ composites, the latter blend containing a liquid crystalline polymer (LCP) and a flexible chain polymer is attractive in two aspects: the LCP acts as a 'processing aid' to reduce the whole melt viscosity [9] and its in situ fibrillation results in a 'self-reinforced' blend [10,11]. These excellent properties strongly depend on the LCP morphology, which is greatly affected by LCP content [12–15], viscosity ratio [12,15], rheological properties [16,17] and processing conditions [12–14]. When additional hydrodynamic effects arise due to the presence of fillers added into in situ composites, the morphological evolution of LCP becomes more attractive, which sometimes is beyond the scope of the understanding of conventional binary blends.

Induced by different fillers, various hydrodynamic factors affect the morphological evolution of LCP in different ways. Tjong and Meng [18] described how the LCP fibrillation was prevented by the lower shear rate resulted from the presence of a higher content of whiskers in polyamide 6 (PA6)/LCP composites. On the other hand, the LCP fibrillation

* Corresponding author. Tel.: +86 10 6261 3251; fax: +86 10 8261 2857.
E-mail address: hejs@iccas.ac.cn (J. He).

0032-3861/$ - see front matter © 2007 Elsevier Ltd. All rights reserved.
doi:10.1016/j.polymer.2007.05.004

promoted by certain contents of glass fiber, glass bead and whisker was investigated for polycarbonate (PC)/LCP, PA6/LCP and polysulfone (PSF)/LCP blends [19–25]. Considering the hydrodynamic effects induced by the added fillers, He and coworkers suggested that LCP melt droplets underwent elongational flow, which favored the LCP fibrillation more effectively than simple shear flow. However, these traditional fillers or fibers made in situ composites much heavier due to their own large density and high loading needed.

Nano-size particulates filled polymers (nanocomposites) are of great interest due to their lower density, excellent performances and attractive prospect, compared to conventionally filled polymers [26,27]. Nano-size fillers such as carbon black (CB) and nano-SiO_2 have been reported to have unique influence on the morphology of immiscible blends such as phase inversion, especially in conductive materials [28–30]. Recently, it has been reported that nano-fillers such as nano-SiO_2 and nano-clay can also act as a compatibilizer in immiscible blends during mixing process [31–37].

However, there are only a few papers dealing with nanoparticle filled in situ composites. Hu et al. [38,39] introduced nano-size fumed silica of different surface properties into the LCP/polypropylene (PP) in situ blends and found that hydrophobic nano-SiO_2 could efficiently promote the fibrillation of LCP droplets. Nano-clay serving as a ''compatibilizer'' in PA6/LCP blends [40] promoted the LCP fibrillation, and nano-SiO_2 through inhibiting the transesterification of LCP and PC enhanced the LCP fibrillation [41]. In these studies, the interfacial effects produced by the nano-filler during melt processing have been emphasized. But the evolution of viscoelastic property of the melt fluid affected by the nano-filler has not been reported. Actually these properties of melt fluid play an important role in determining the evolution of flow field, especially the flow in complex geometries. The development of vortex phenomenon, when the melt flows through an abrupt contraction, is caused by the stress field exerted by the fluid because of its viscoelastic characters. In fact, the relation between viscoelastic property of melt fluid and flow field has been reported by several researchers [42–45]. They suggested that fluid elasticity was responsible for the vortex enhancement and the evolution of stress field. Moreover, our previous study [25] showed that the aspect ratio of whiskers affected the hydrodynamic effect in the entrance zone of capillary die due to the difference of viscoelasticity. Therefore, does the addition of nano-filler affect the viscoelastic property of filled in situ composites? How do the viscoelastic properties of these ternary systems affect the evolution of LCP morphology? The answers to these questions are still unclear. A deeper understanding of these phenomena will correlate the morphological development with viscoelastic property of multicomponent blends more closely.

In the present work, two series of binary and ternary blends were prepared by adding small amounts of LCP and different contents of nano-SiO_2 into polysulfone (PSF). The rheological properties of PSF, LCP and corresponding blends were measured with the help of capillary rheometry and parallel plate rheometry, and the morphology of LCP was observed on a scanning electron microscope. The morphological evolution of LCP was investigated in the presence of various contents of nano-SiO_2, and especially correlated to the sharp increase of elasticity caused by nano-SiO_2.

2. Experimental

2.1. Materials

Polysulfone (PSF) with an intrinsic viscosity of 0.54 dl g^{-1}, produced by Shanghai Shuguang Chemical Factory, China, was used as the matrix. The LCP used was commercial thermotropic liquid crystalline copolyester (Vectra B950, Hoechst Celanese, USA), comprising of hydroxynaphthoic acid (HNA), aminophenol (AP) and terephthalic acid (TA), hereafter referred to as VB. The nano-size fumed silica (Aerosil R974) was purchased from Degussa Co., Germany. Surface modification of the silica with 1,1-dimethyl dichlorosilane was already performed by the manufacturer. More detailed physical properties of the nano-SiO_2 are listed in Table 1.

2.2. Blending

Prior to melt blending, all the materials were dried at 120 °C under vacuum for at least 24 h. To obtain a better dispersion of nano-SiO_2 in the PSF matrix, PSF/SiO_2 mixtures were pre-extruded, pelletized and well dried, followed by re-blending with or without LCP. The melt blending was conducted on a Haake twin-screw extruder (TW100) equipped with a pair of counter-rotating intermeshing cone-shaped screws. A temperature profile of 260–305–305–300 °C from hopper to die was imposed. The screw speed was 60 rpm. The extrudates were quenched by water, pelletized and well dried, followed by blending with LCP using a Haake rheomix 600 equipped with rotors. The blending temperature was 305 °C and the rotating speed was 50 rpm. The total blending time was 10 min. Two fixed PSF/LCP ratios of 90/10 and 95/5 were adopted for all the blends, and the nano-SiO_2 content was taken as 0, 1, 3 and 5 vol%.

2.3. Rheological measurement

The steady shear rheological property of all the pure components and blends were measured at 290 °C using a Rosand twin-bore advanced capillary rheometer, model RH7 (Bohlin Instruments Ltd., UK). The rheometer was equipped with two 1-mm capillary dies (a zero-length die and a 16-mm length die) to carry out the Bagley correction for the end effects. The entry angle of die was 180°. According to the

Table 1
Physical properties of nano-SiO_2 R974

Density (g/cm^3)	BET surface area (m^2/g)	Average primary particle diameter (nm)	Surface property	Purity (wt% of silica)
2.0	170 ± 20	12	Hydrophobic	>99.8

operation procedure of this capillary rheometer, the shear viscosity, extensional viscosity, extension rate and extensional stress were measured directly. The extrudates at studied plunger speeds (i.e., different shear rates) were collected without any post-drawing for further morphological analysis.

Dynamic shear rheological measurements were carried out on a Rheometrics SR 200 dynamic stress rheometer, using a 25-mm parallel plate geometry and a 1-mm sample gap. The samples were injection molded at 305 °C into 1-mm thick plates by using a CS-183 Mini-Max Molder (CSI, Cedar Knolls, NJ, USA), and then cut into small disks of about 25 mm in diameter. Before rheological measurements, samples were dried in a vacuum oven at 120 °C for 24 h to remove the moisture. Samples were placed between the preheated plates and were allowed to equilibrate for 10 min prior to the test. The dynamic viscoelastic properties were determined with frequencies from 0.1 to 100 rad/s, by using strain values determined with a stress sweep to lie within the linear viscoelastic region. To study the linear viscoelastic properties at low frequencies, the oscillatory shear measurements were performed at a relatively small strain amplitude ($0.01 < \gamma_0 < 0.03$). In each measurement, it was possible to apply sufficient strain amplitudes (and still remain in the linear viscoelastic regime) to ensure adequate torque values. All measurements were carried out in nitrogen atmosphere at 290 °C.

2.4. Morphological observation

The extrudates from capillary rheometer were cryofractured in liquid nitrogen and sputter-coated with gold. Then, the fracture surface was observed by using a scanning electron microscope (SEM, Hitachi S-4300, Japan). To clearly show the LCP particles, the collected extrudates were immersed in *N*,*N*-dimethylacetamide (DMAc) for at least 24 h to dissolve the PSF matrix in the first step, followed by repeated washing of the residue with fresh solvent. The residue LCP was coated with a thin layer of gold and observed on a scanning electron microscope. Software, Phototshop 6.0 was used to measure the long axis a and the short axis b of LCP rods and fibrils. Consequently the aspect ratio λ was given by $\lambda = a/b$.

3. Results and discussion

3.1. Formation of long LCP fibrils

The morphological observation was carried out for two series of samples loaded with fixed PSF/VB ratios at 95/5 and 90/10, respectively, and different nano-SiO_2 contents. These samples were extruded from a capillary rheometer at the shear rate of $\sim 100\ s^{-1}$. From Fig. 1a obtained for the unfilled PSF/VB 95/5 blend, it was found that VB particles were

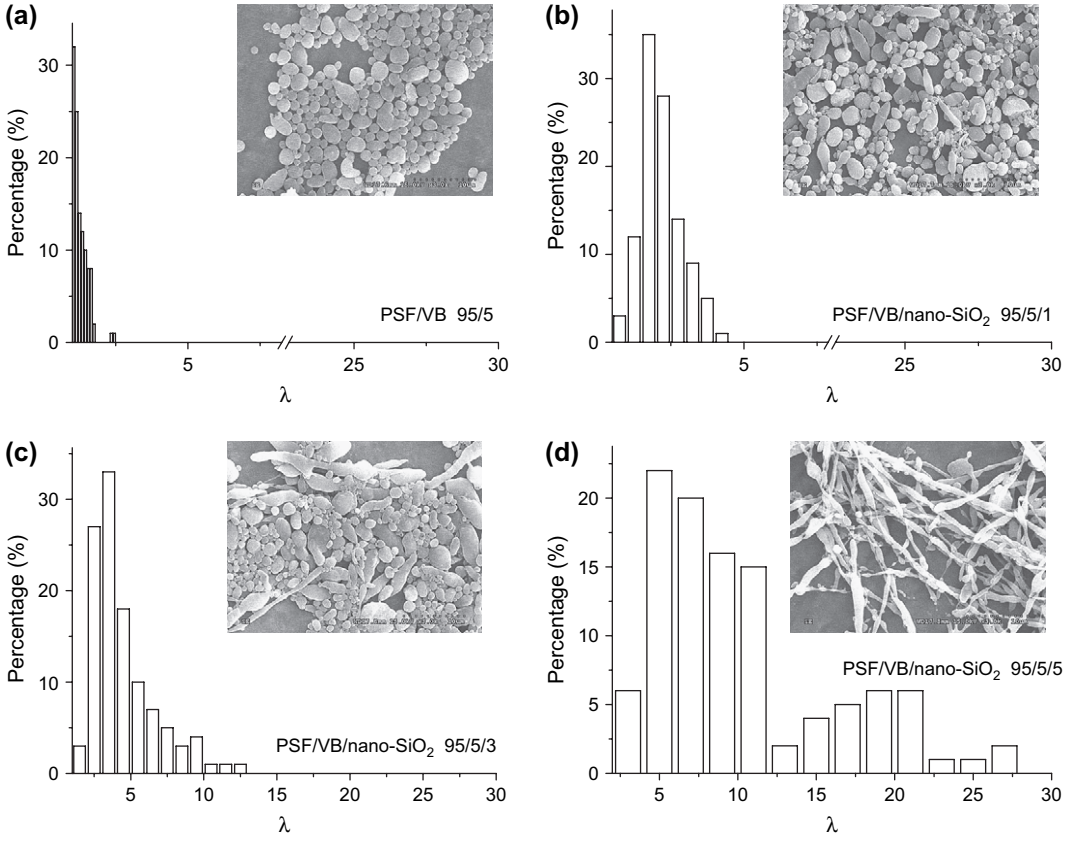

Fig. 1. SEM micrographs of residues extracted from the blends together with corresponding aspect ratio distribution of VB particles, the weight ratio of PSF/VB in the blends is always 95/5 and nano-SiO_2 content is: (a) 0 vol%, (b) 1 vol%, (c) 3 vol%, (d) 5 vol%.

spherical or ellipsoidal in shape. A previous study [7] showed that for PSF/LCP binary system, the LCP fibrillation took place only at the viscosity ratio below 0.01. However, in the present study the viscosity ratio of the dispersed VB phase to the PSF matrix was 0.08, eight times of 0.01. It means that the viscosity ratio was not small enough to cause the deformation of the dispersed VB droplets. Then if the capillary number is considered as a criterion for the deformation of dispersed droplets in the matrix, the ratio of $Ca/Ca_c > 4$ is needed for an affine deformation and fibril formation [46], so do for the deformation and fibrillation of LCP melt droplets [47]. However, under the present conditions, the capillary number and the critical capillary number were 22.3 and 6.3, respectively, i.e., Ca/Ca_c was about 3.5. It means that the capillary number was not large enough, as $Ca \gg Ca_c$, to cause the LCP fibrillation. In addition, the interfacial adhesion between PSF and LCP was relatively too poor to transfer the shear stress effectively from the matrix to LCP droplets for LCP deformation. Next to Fig. 1a, the statistic value of aspect ratio indicates that less than 9% of VB droplets were deformed into ellipsoids in the binary PSF/VB blend. However, with nano-SiO_2 added in concentration of 1 and 3 vol%, there are some stretched LCP particles in Fig. 1b and c. It is clear that the introduction of nano-SiO_2 into PSF/VB blends promoted the deformation of dispersed VB droplets into rods and fibrils having larger aspect ratios.

It is interesting to find out that a sharp increase of aspect ratio of VB particles appeared at the 5 vol% nano-SiO_2 content (Fig. 1d). At this composition the average aspect ratio of VB significantly increased to 10.3 with the maximum value of 27, which has never been reported at such low LCP content and such low shear rate.

In order to further illustrate this interesting phenomenon, the other series of PSF/VB 90/10 blends loaded with different nano-SiO_2 contents were investigated too. The morphology of VB particles extracted from these composites is shown in Fig. 2, together with the aspect ratio distribution of VB particles. For binary PSF/VB blend (Fig. 2a), the aspect ratio of 96% VB particles is smaller than 2. With the introduction of nano-SiO_2 (Fig. 2b and c), more well-developed VB fibrils were obtained. More importantly, a great increase of aspect ratio of VB particles also appeared at 5 vol% nano-SiO_2 content. At this content, very long VB fibrils were observed both in the fractured (Fig. 2d) and the residue extracted from the PSF matrix (Fig. 2e and f). These long VB fibrils perfectly align along the same direction, suggesting that the VB droplets undertook a large stress in the same direction of flow. The diameter of long VB fibrils ranged from 1.8 to 4.1 μm. However, their exact length could not be determined, because these fibrils extend out the view field even at a quite low magnification of 500×. This was the reason why it was failed to supply a plot to show the aspect ratio distribution of VB fibrils. Anyway, from the estimation even the shortest VB fibrils were longer than 100 μm. This means that the average aspect ratios of VB fibrils were at least larger than 30. These results clearly show that the presence of nano-SiO_2 promoted the fibrillation of VB droplets in the PSF matrix in capillary flow. Especially, very long LCP fibrils with average aspect ratios larger than 30 were formed in blends containing nano-SiO_2 of 5 vol%.

Such a structure having quite long LCP fibrils is usually formed at high LCP contents [48–52], obtained by hot drawing [51,53,54] or by co-extrusion [55]. In the present study, the PSF/VB/nano-SiO_2 composites had LCP content lower than 9.2 wt% and the shear rate about 100 s^{-1} only, and furthermore, with neither hot drawing nor co-extrusion to avoid any post-drawing during sampling. Based on the experience, it seems impossible to make LCP to deform into these perfectly oriented long fibrils in the present samples.

3.2. Factors influencing the morphology of LCP

From the above results, it would be interesting to find out the factors influencing the formation of these long VB fibrils. The morphology of an immiscible polymer blend is closely correlated with its rheology. Therefore, the rheological properties of the blends were studied first. Fig. 3 shows flow curves of PSF, PSF/VB blend, and PSF/VB/nano-SiO_2 composites containing 10 wt% VB and various contents of nano-SiO_2, measured with the capillary rheometer at 290 °C. In order to find out if the viscosity ratio was the dominant factor influencing the LCP fibrillation in ternary PSF/VB/nano-SiO_2 composites, the calculation of viscosity ratio and capillary number was conducted. The values of interfacial tension of possible PSF–VB, PSF–SiO_2 and VB–SiO_2 pairs were 0.5, 11.6 and 14.1 mN/m, respectively. From these data it was clear that nano-silica was distributed selectively in the PSF matrix so that its addition increased the viscosity of the matrix and decreased the viscosity ratio as shown in Table 2. However, the viscosity ratios were not small enough to result in the deformation and fibrillation of LCP droplets in this ternary system. We will further discuss this point from the capillary number. From Eq. (1) [56], the capillary number, Ca, is defined as the ratio of the shear stress acting on the VB droplet by an external flow field to the interfacial tension resisting the deformation of the spherical droplet.

$$\mathrm{Ca} = \frac{\eta_b \dot{\gamma} d\left[1-(4\phi_d\phi_m)^{0.8}\right]}{2\sigma}\frac{16p+16}{19p+16} \tag{1}$$

where η_b is the blend viscosity, $\dot{\gamma}$ is the shear rate, d is the diameter of the dispersed phase droplet and can be calculated according to the method of our previous paper [24], σ is the interfacial tension, p is the viscosity ratio, ϕ_d is the volume fraction of the dispersed phase, and ϕ_m is the volume fraction of the matrix. By using Eq. (1) the values of capillary number of the present system were calculated and listed in Table 2. It shows that the capillary number of PSF/VB/nano-SiO_2 composites increased with increasing nano-SiO_2 content. This means that the deformation of VB droplets would have become easier with the introduction of nano-SiO_2 through decreasing the viscosity ratio. However, the increase in Ca with the increase of nano-SiO_2 content was very small. As the nano-SiO_2 content increased from 3 to 5 vol%, the capillary number changed from 29.3 to 30.2. This small increase of

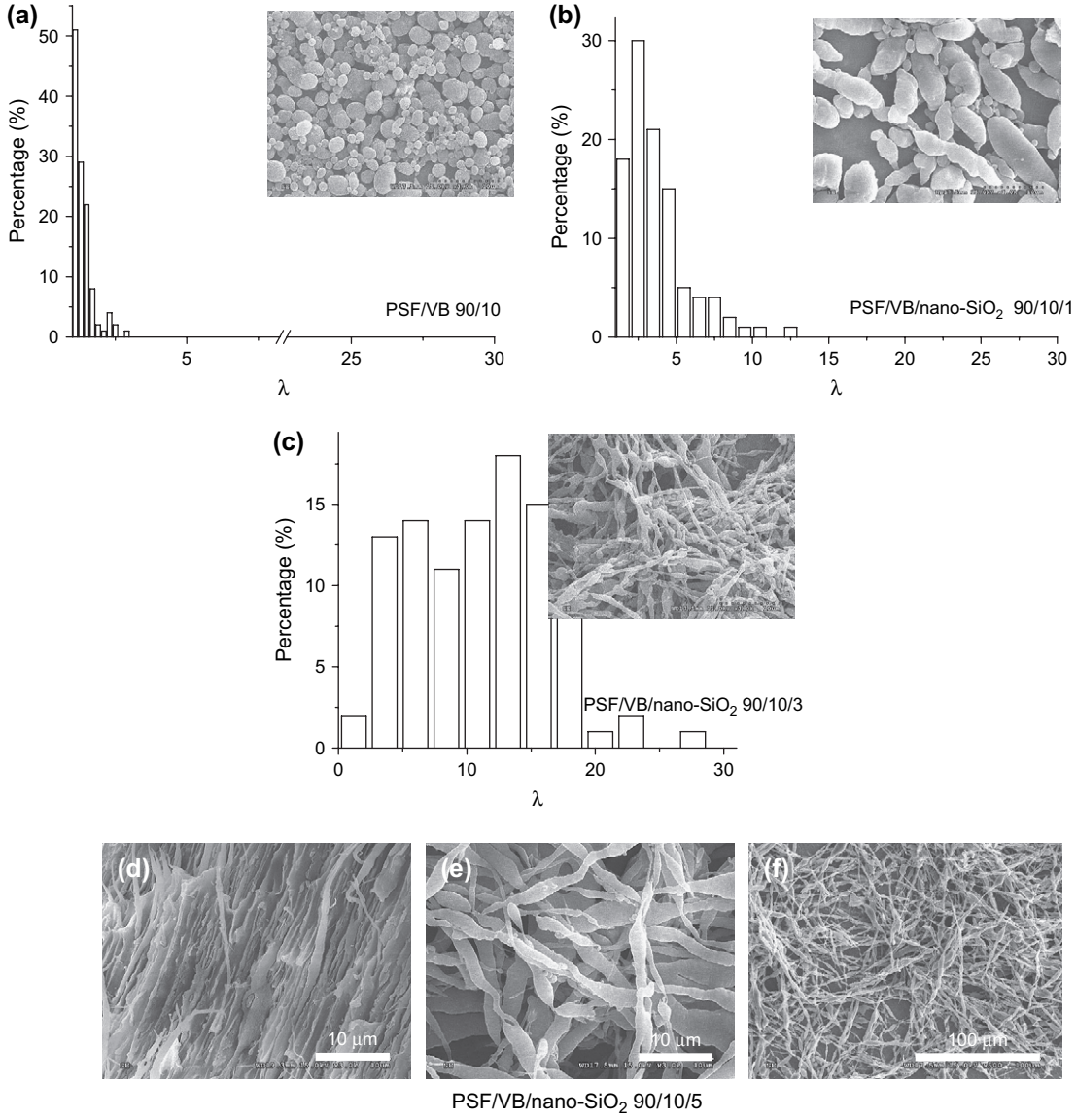

Fig. 2. SEM micrographs of cryogenically fractured and residues extracted from the blends together with corresponding aspect ratio distribution of VB particles, the weight ratio of PSF/VB in the blends is always 90/10 and nano-SiO_2 content is: (a) 0 vol%, (b) 1 vol%, (c) 3 vol%, (d), (e) and (f) 5 vol%; (d) cryofractured surface parallel to the main flow direction; extracted residue under (e) higher magnification (×3000) and (f) lower magnification (×500).

only 3% could not increase the average aspect ratio of VB about three- to five-fold. Therefore, if the viscosity ratio of VB to the matrix was one of the factors influencing the LCP fibrillation, then it was not the predominant factor determining the fibrillation of VB in the present system, similar to the results reported for PSF/VA/whisker systems [24].

Furthermore, the fact that the addition of nano-SiO_2 promoted the fibrillation of LCP has been reported for a polycarbonate/nano-SiO_2/LCP system [41]. Wu and his coworkers proposed that through inhibiting the transesterification of LCP and polycarbonate (PC), nano-SiO_2 enhanced the fibrillation of LCP. However, in the presently studied polysulfone/VB/nano-SiO_2 systems, PSF and VB were incompatible and their transesterification reaction was insignificant. DSC heating curves of PSF/VB/nano-SiO_2 system are shown in Fig. 4, where the T_g of the PSF phase changes little with the addition of VB and nano-SiO_2. Therefore, there must be other strong factors governing the significant fibrillation of VB phase rather than the inhibited transesterification.

3.2.1. Effect of nano-SiO_2 on viscoelastic property

The signature of microstructure of bi-phase or multi-phase systems can be obtained through investigating the dynamic rheological property in the linear viscoelastic region [57–67]. In addition, the storage (elastic) modulus (G') is more sensitive to the evolution of microstructure. Therefore, using the G' value to characterize the microstructure existing in the system is a convenient approach broadly applied by many researchers [57,61–67].

Fig. 5 shows a comparison of storage (elastic) modulus (G') and loss modulus (G'') for PSF and PSF/nano-SiO_2 composites containing various contents of nano-SiO_2, measured with a

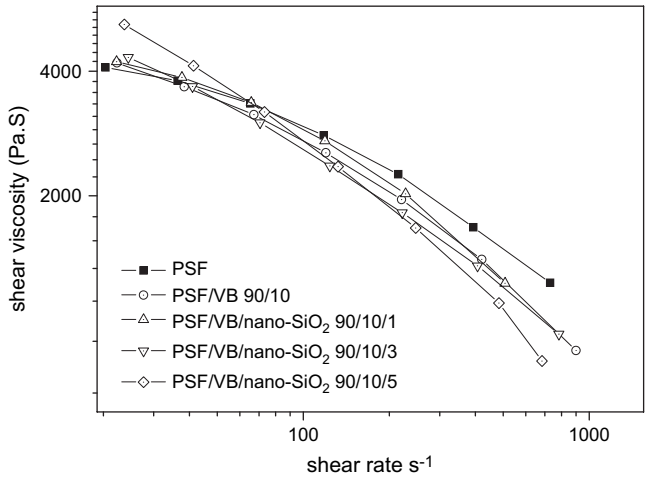

Fig. 3. Viscosity of PSF, PSF/VB and PSF/VB/nano-SiO_2 composites as a function of shear rate.

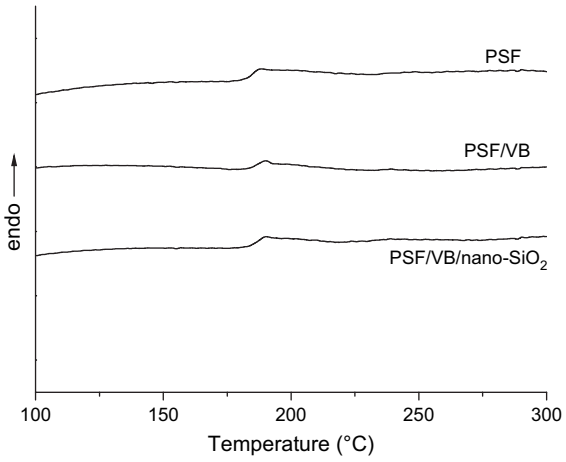

Fig. 4. DSC heating curves for PSF/VB/nano-SiO_2 system.

parallel plate rheometer. As shown in this figure, G' increases with increasing nano-SiO_2 content and the measurement frequency. With nano-SiO_2 introduction up to 3 vol% into PSF matrix, G' of the system increases slightly and the slope of terminal region changes gradually, showing that the system kept a relatively good dispersion of silica. With further addition of nano-SiO_2 up to 5 vol%, the G' value increases sharply with an increment of about two orders of magnitude. At this content, the system displayed a solid-like behavior, indicating that a nano-SiO_2 network formed in the system at some extent. In addition, at the silica content of 5 vol% the G'' crosses over the G', indicating near the gel point at this composition [68].

Fig. 6 shows the variation of G' as a function of angular frequency of the pure PSF, PSF/VB blends and nano-SiO_2 filled systems. As shown in Fig. 6a, the curves of PSF/VB 95/5 and 90/10 move up almost parallel to the PSF one, indicating that the VB content has little influence on G' value. However, the G' value has a strong dependence on the content of nano-SiO_2, as shown in Fig. 6b and c. Compared with the binary PSF/VB blend, the low-frequency G' of ternary PSF/VB/SiO_2 system did not increase distinctly with lower SiO_2 content (1–3 vol%), while it is enhanced by about two orders of magnitude with silica loading at 5 vol%. It means that the elasticity of PSF/VB/SiO_2 samples was still dominated by the binary PSF/VB blend matrix in lower nano-SiO_2 loadings, while the elasticity experienced a transition from liquid-like behavior to solid-like one at SiO_2 loading of 5 vol%. Fig. 6b and c also gives the G'' of ternary PSF/VB/SiO_2 systems, and shows the similar trend with the PSF/nano-SiO_2 composites, that is, the silica content of 5 vol% is at the gel point. These results indicate that the addition of nano-SiO_2 had a significant effect on the linear dynamic viscoelastic response of these samples, especially in the low-frequency region.

To further study the effect of nano-SiO_2 content on the dynamic rheological behavior, the dependence of G' enhancement in low-frequency range on the nano-SiO_2 loading was investigated and shown in Fig. 7. It is clearly shown that lower nano-SiO_2 content affected G' a little. However, the nano-SiO_2 content up to 5 vol% resulted in a sharp increase of G'. The nano-SiO_2 content played an important role in determining G' of these ternary systems.

Li et al. [69] have considered that the contribution of nano-filler to G' of the nanocomposites (G'_{comp}) can be analyzed in terms of two effects: the confinement effect (G'_{conf}) and the interparticle interactions (G'_{inter}), which result in the enhancement of low-frequency G' in comparison with the polymer matrix (G'_{matrix}), i.e.,

$$G'_{comp} = G'_{matrix} + G'_{conf} + G'_{inter} \quad (2)$$

here G'_{conf} arises from the confinement of nano-filler with a diameter smaller than or of the same order of the size of the

Table 2
Effect of nano-SiO_2 content on the viscosity ratio of the VB to PSF/nano-SiO_2 composites and capillary number of PSF/VB/nano-SiO_2 composites at a shear rate of 100 s^{-1} and the weight ratio of PSF/VB in the blends is 90/10

Nano-SiO_2 content (vol%)	0	1	3	5
Viscosity ratio	0.08	0.07	0.06	0.055
Capillary number	22.3	26.1	29.3	30.2

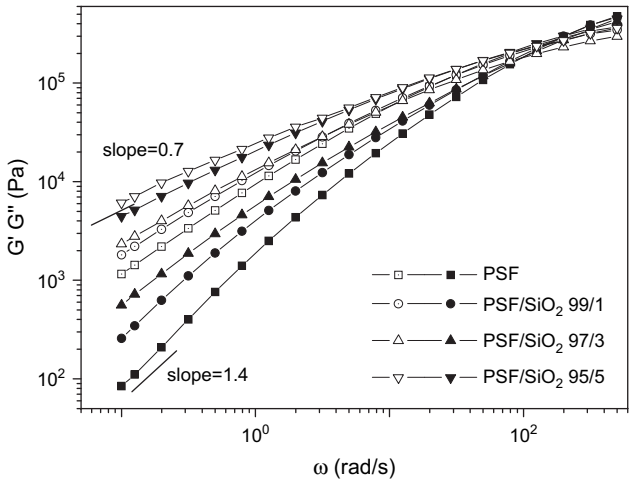

Fig. 5. Effect of nano-SiO_2 content on complex shear modulus of PSF/nano-SiO_2 composite. G': full symbol and G'': empty symbol.

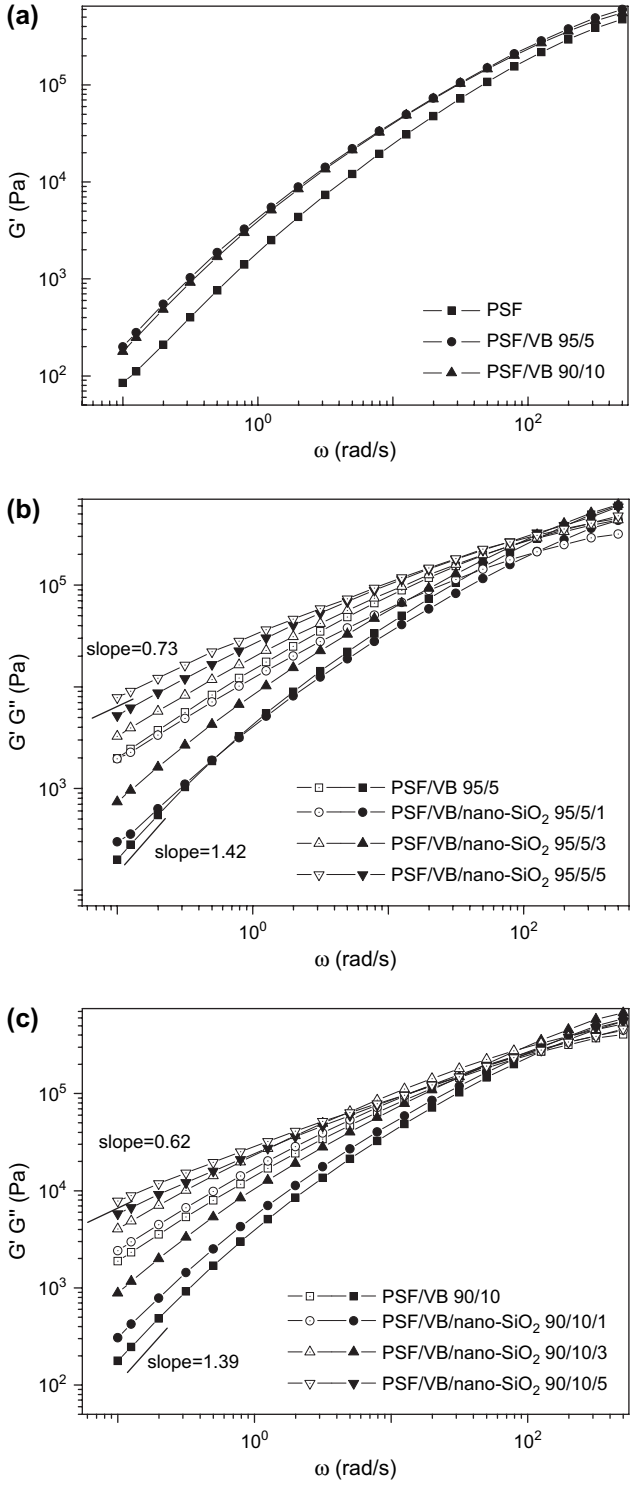

Fig. 6. Comparison of complex shear modulus for binary PSF/VB blend and ternary PSF/VB/SiO_2 system containing various contents of nano-SiO_2. G': full symbol and G'': empty symbol.

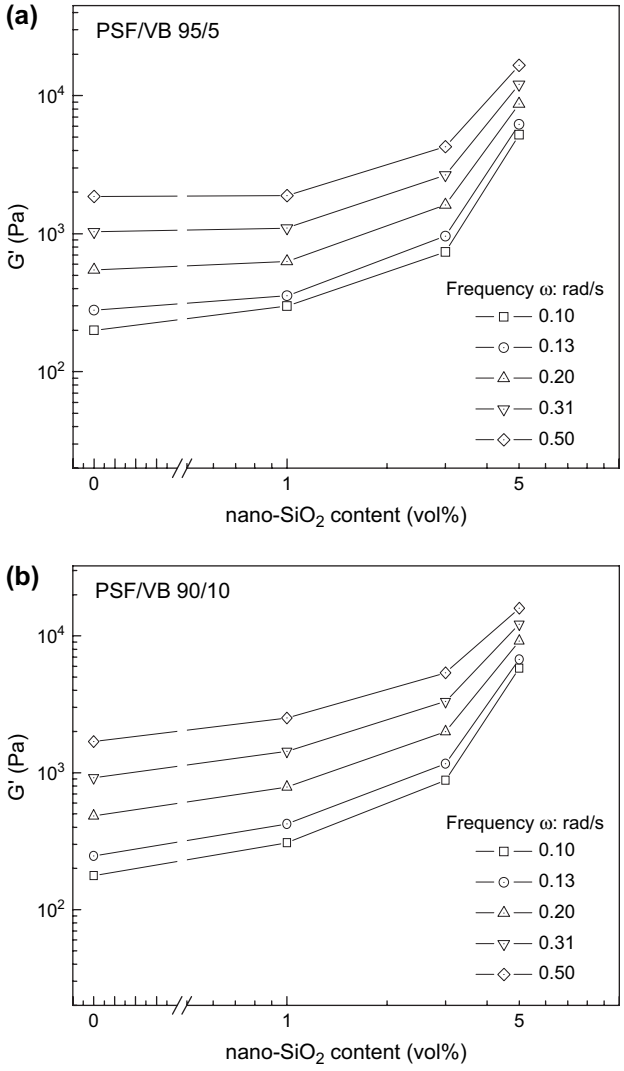

Fig. 7. Dependence of storage modulus on nano-SiO_2 content for ternary PSF/VB/SiO_2 systems with PSF/VB ratio at: (a) 95/5 and (b) 90/10 at low frequency.

chain coils that may lead to the alternation of the relaxing dynamics of the confined polymers [70]. G'_{inter} comes from frictional interactions between nano-fillers. G'_{comp} may be dominated by G'_{inter}, because the contribution of G'_{inter} is much larger than those of G'_{matrix} and G'_{conf} at low frequencies. These interactions can greatly increase when the filler loading is above a percolation threshold, which may lead to the significant enhancement of low-frequency G'. Therefore, in the present study the small contribution of G'_{inter} at nano-SiO_2 content lower than 3 vol% indicated that the nano-SiO_2 content was still below the percolation limit. However, the low-frequency G' enhanced sharply when the nano-SiO_2 loading was up to 5 vol%, which obviously resulted from the physical jamming of nano-fillers.

From the above discussion, we know that the addition of nano-SiO_2 had a significant effect on the elasticity of blends. Their elasticity increased with increasing nano-SiO_2 content, and the great increase of elasticity appeared at the 5 vol% content. Due to the influence of rheological properties on the morphology, this sharp increase of elasticity may be responsible for the formation of the long VB fibrils in our system studied.

3.2.2. Influence of nano-SiO_2 on decrease of entrance angle

It is widely accepted that the elongational flow developed at the entry of the capillary is mainly responsible for the LCP

fibrillation during a capillary extrusion. Now the discussion should move to a further question: how did the introduction of nano-SiO_2 alter the elongational flow field? The theory predicting the converging flow leading to the vortices also involves their relationship to elastic property [42]. Some researchers suggested that fluid elasticity was responsible for the vortex enhancement [43–45]. However, no visual method can detect the phenomenon of vortex enhancement. Fortunately, the evolution of entrance angle of capillary has been obtained by using the analyses of Cogswell and Binding on the entrance region of capillary.

Cogswell [71,72] has considered the flow in the converging region as consisting of successive coni-cylindrical region of differential length, whose geometry is such that the pressure drop is a minimum. In each coni-cylindrical region, Poiseuille flow is assumed. After mathematical analysis, the following equation can be derived.

$$\Delta P_0 = \left[\left\{ 2\frac{4^{3t+1}}{3^{t+1}} \xi k^t \left(\frac{n}{3n+1} \right)^{2t} \right\}^{1/(1+t)} \frac{1}{n+1} \right] \gamma^{t(1+n)/t+1} \tag{3}$$

where ξ, t, k and n are the power-law parameters that characterize the shear and elongational viscosities.

Then the angle between the converging stream and the longitudinal axis of the capillary entrance, θ, can be calculated by means of the following equation:

$$\tan\frac{\theta}{2} = \frac{\varepsilon}{\gamma_a} \tag{4}$$

where ε, the average extension rate, can be obtained from the ΔP_0, pressure drop in the converging flow region, and the related equation [73], and γ_a is the apparent shear rate.

Binding [74] has assumed that the fluid follows the power-law expressions. His analysis also considers the completely developed flow in the converging region, but as different from Cogswell's analysis, the velocity profiles and strain rates used always correspond to power-law fluids. After minimizing the viscous energy dissipation in the converging region, the following equation is obtained:

$$\Delta P_0 = \left[\frac{2k(1+t)^2}{3t^2(1+n)^2} \left\{ \frac{\xi t(3n+1)n^t I}{k} \right\}^{1/(1+t)} \right] \gamma^{t(1+n)/t+1} \tag{5}$$

$$I = \int_0^1 \left| 2 - \left(\frac{3n+1}{n} \right) \phi^{1+(1/n)} \right| \phi \mathrm{d}\phi \tag{6}$$

and correspondingly, the entrance angle is given by the following equation.

$$\tan\theta = \frac{2(n+1)}{3n+1} \frac{\varepsilon}{\gamma_a} \tag{7}$$

In the present study, both Cogswell and Binding analyses were adopted to calculate the entrance angle of nano-SiO_2 filled PSF/VB blends. The elongational behavior of the polymer was obtained from the data of pressure drop in the converging flow region in the entrance zone of a capillary die. Calculated with Eqs. (4) and (7), the value of entrance angle of PSF/VB and PSF/VB/nano-SiO_2 blends are shown in Fig. 8a and b, respectively. Fig. 8a presents the entrance angle of PSF/VB blends containing 0, 1, 3, and 5 vol% nano-SiO_2 according to Binding's analysis. These samples had fixed PSF/VB ratios at 90/10 and 95/5, and were extruded from a capillary rheometer at the shear rate $\sim 100\ s^{-1}$. For the unfilled PSF/VB blend, the entrance angle was 10.5°, suggesting a relatively small vortex in the converging flow region at the entry of capillary. The addition of 3 vol% nano-SiO_2 decreased θ to 8.8°, i.e., a decrease of 12%, while 5 vol% nano-SiO_2 decreased θ to 5.6°, i.e., a decrease of 36%. With the increase of nano-SiO_2 loading into the PSF/VB blend, for both 90/10 and 95/5 systems, the entrance angle decreased gradually, and at the content of 5 vol% it showed a sharp decrease. That is to say, the vortex in the converging flow region at the entry of capillary was reduced with the addition of nano-SiO_2 and decreased sharply at the nano-SiO_2 content up to 5 vol%. This was in line with the variation of viscoelastic property of materials, in which fluid elasticity was responsible for the vortex enhancement [43–45]. Fig. 8b shows a trend similar to that

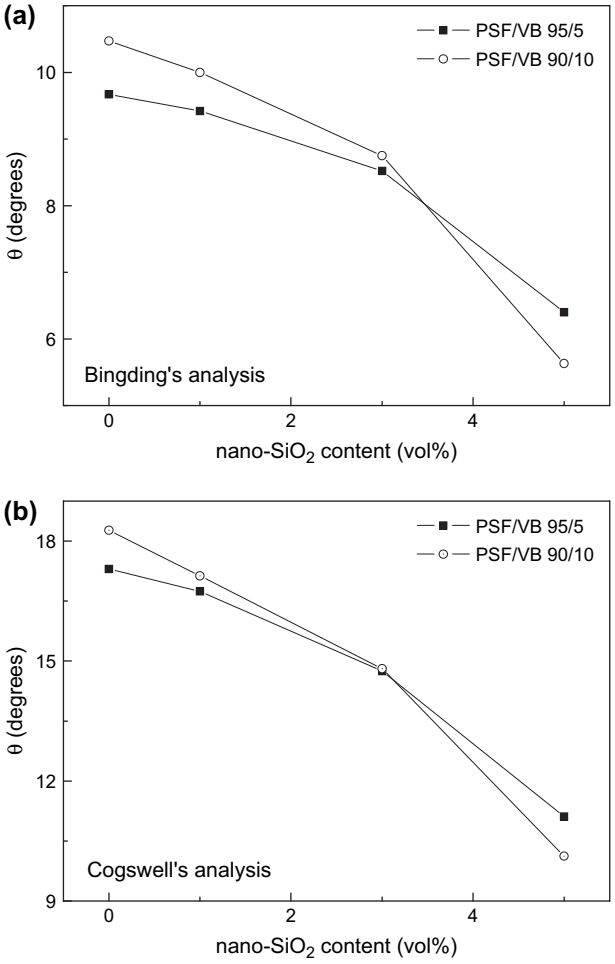

Fig. 8. Plot of entrance angle (θ) at the entrance of capillary die vs. the volume fraction of nano-SiO_2 at the shear rate of 100 s^{-1}, according to (a) Binding's analysis and (b) Cogswell's analysis.

exhibited in Fig. 8a. Although the values of entrance angles according to Cogswell and Binding methods were different, the tendency of evolution was quite similar, that is, the θ decreased with increasing nano-SiO_2 content. Both methods predicted a decreasing entrance angle as a function of nano-SiO_2 content, thus indicating the vortex growth.

3.2.3. The increase of elongational field promoting the fibrillation of LCP

The phenomenon of vortex enhancement in the converging flow region at the entry of capillary is the key issue to understand the evolution of the flow field [24,25]. The vortex enhancement, once generated, results in the enlargement of the acceleration zone and the increase of fluid velocity, which in turn increase the strength of the elongational field and the elongational stress in the entrance of capillary.

The plot of elongational stress vs. the volume fraction of nano-SiO_2 at the shear rate of 100 s^{-1} is shown in Fig. 9 for the two series of system at PSF/VB ratios of 90/10 (a) and 95/5 (b). For comparison, the average aspect ratio of VB particles is also shown. In Fig. 9a, the shadowed area with the dot lines represents the estimated average aspect ratio due to the same reason for Fig. 2d–f. It is clearly shown that the elongational stress of entrance region of capillary increases significantly with increasing nano-SiO_2 content. Compared with our previously studied PSF/LCP/whisker system, the nano-SiO_2 system showed more pronounced increase of the stress. For example, the addition of 11.5 vol% of calcium carbonate and aluminum borate whiskers increased the elongational stress to 1180 and 1580 kPa, respectively. However, the relatively smaller amount of nano-SiO_2 addition, i.e., 5 vol%, generated 1950 kPa stress in the converging flow region at the entry of capillary. Like the profile of entrance angle, the elongational stress of ternary PSF/VB/nano-SiO_2 blends was also dramatically increased when the nano-SiO_2 content was up to 5 vol%. This more pronounced extra elongational stress is most probably ascribed to the network formed by nano-SiO_2 filler and resultant sharp increase of G'.

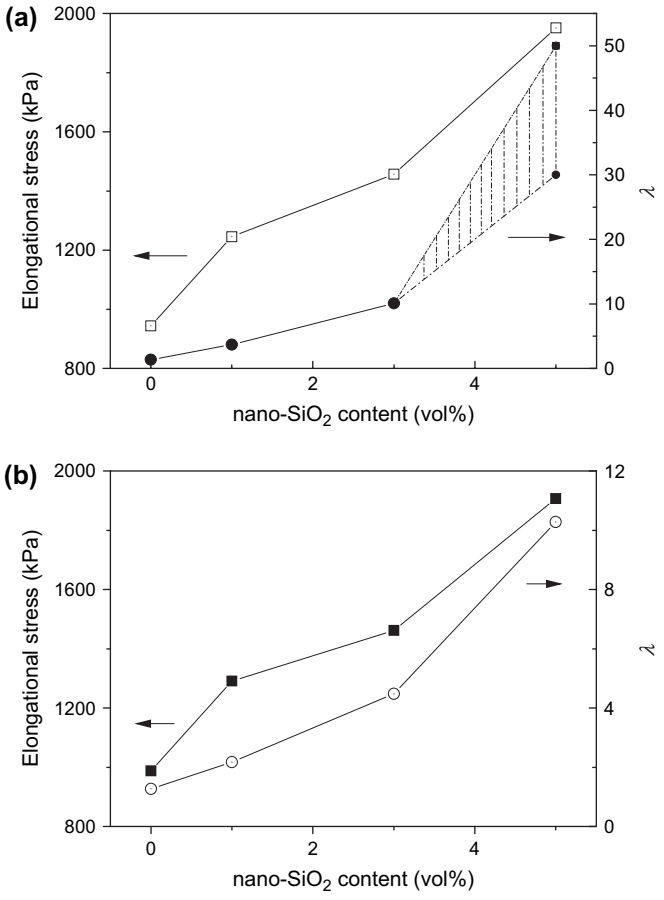

Fig. 9. Plot of the elongational stress of binary PSF/VB blends and ternary PSF/VB/SiO_2 blends at different nano-SiO_2 contents, with PSF/VB ratio at: (a) 90/10 and (b) 95/5.

Correspondingly the average aspect ratio of VB increases with the increased elongational stress in the converging flow region in the entrance zone of a capillary die (Fig. 9). It is known that the elongational flow is the most favorable flow field to promote the LCP fibrillation in in situ composites [75]. Except for this, LCP fibrils formed probably relaxed after entering the capillary. However, the deformed droplets relaxed much more slowly in high elastic matrix [76] and so did in the filled-PSF matrix of the present study. In addition, the deformable phase was LCP having very longer relaxation time due to the rigidity of its molecular chains. Therefore, the fibrillar morphology of LCP remained after leaving the capillary. So with the introduction of nano-SiO_2 into PSF/VB blends, the extra elongational stress was the predominant factor to promote the VB fibrillation and increase the average aspect ratio of VB over 30.

4. Conclusions

This paper presents the morphological evolution of LCP promoted by the network formed by higher content of nano-SiO_2 in PSF matrix. Quite long and perfectly oriented VB fibrils were obtained in the more pronounced elongational field, where VB melt droplets were deformed, stretched and stabilized when entering the capillary. The greatly increased elongational stress together with reduced entrance angle and enhanced vortex was ascribed to the dramatically increased elasticity of ternary PSF/VB/SiO_2 system due to the network formed by nano-SiO_2 filler. This reveals that the extra elongational stress was the directly predominant factor to generate these long and perfectly oriented VB fibrils in PSF/VB/SiO_2 system.

Acknowledgements

This work was supported by the National Nature Science Foundation of China, Grant No. 50233010.

References

[1] Favis BD, Chalifoux JP. Polym Eng Sci 1987;27:1591–600.
[2] Favis BD, Chalifoux JP. Polymer 1988;29:1761–7.

[3] Favis BD. J Appl Polym Sci 1990;39:285–300.
[4] Wu S. Polym Eng Sci 1987;27:335–43.
[5] Min K, White JL, Fellers JF. Polym Eng Sci 1984;24:1327–36.
[6] Beery D, Kenig S, Siegmann A. Polym Eng Sci 1991;31:451–8.
[7] He J, Bu W, Zhang H. Polym Eng Sci 1995;35:1695–704.
[8] Utracki LA. J Rheol 1991;35:1615–37.
[9] Weiss RA, Huh W, Nicolais L. Polym Eng Sci 1987;27:684–91.
[10] Kiss G. Polym Eng Sci 1987;27:410–23.
[11] Lee HS, Fishman D, Kim B, Weiss RA. Polymer 2004;45:7807–11.
[12] Tan LP, Yue CY, Tam KC, Lam YC, Hu X. Polym Int 2002;51:398–405.
[13] Saengsuwan S, Mitchell GR, Bualek-Limcharoen S. Polymer 2003;44: 5951–9.
[14] Filipe S, Cidade MT, Wilhelm M, Maia JM. Polymer 2003;45:2367–80.
[15] Van Eijndhoven-Rivera MJ, Wagner NJ, Hsiao B. J Polym Sci Part B Polym Phys 1998;36:1769–80.
[16] Guido S, Simeone M, Greco F. Polymer 2003;44:467–71.
[17] Lee MW, Hu X, Yue CY, Li L, Tam KC, Nakayama K. J Appl Polym Sci 2002;86:2070–8.
[18] Tjong SC, Meng YZ. Polymer 1999;40:1109–17.
[19] Chen P, Wu L, Ding Y, Zhang J, He J. Compos Sci Technol 2006;66: 1564–74.
[20] Chen P, Chen J, Zhang B, Zhang J, He J. J Polym Sci Part B Polym Phys 2006;44:1020–30.
[21] Chen P, Zhang J, He J. Polymer 2005;46:7652–7.
[22] Ding Y, Zhang J, Chen P, Zhang B, Yi Z, He J. Polymer 2004;45: 8051–8.
[23] Zheng X, Zhang J, He J. J Polym Sci Part B Polym Phys 2004;42: 1619–27.
[24] Chen J, Chen P, Wu L, Zhang J, He J. Polymer 2006;47:5402–10.
[25] Chen J, Chen P, Wu L, Zhang J, He J. Int Polym Proc 2007;22:166–72.
[26] Ray SS, Okamoto M. Prog Polym Sci 2003;28:1539–641.
[27] Rong MZ, Zhang MQ, Zheng YX, Zeng HM, Friedrich K. Polymer 2001; 42:3301–4.
[28] Steinmann S, Gronisk W, Friedrich C. Polymer 2002;43:4467–77.
[29] Gubbels F, Blacher S, Vanlathem E, Jerome R, Deltour R. Macromolecules 1995;28:1559–66.
[30] Gubbels F, Jerome R, Vanlathem E, Deltour R, Blacher S, Brouers F. Chem Mater 1998;10:1227–35.
[31] Zhang Q, Yang H, Fu Q. Polymer 2004;45:1913–22.
[32] Vermant J, Cioccolo G, Nair KG, Moldenaers P. Rheol Acta 2004;43: 529–38.
[33] Wang Y, Zhang Q, Fu Q. Macromol Rapid Commun 2003;24:231–5.
[34] Voulgaris D, Petridis D. Polymer 2002;43:2213–8.
[35] Khatua BB, Lee DJ, Kim HY, Kim JK. Macromolecules 2004;37: 2454–9.
[36] Ray SS, Pouliot S, Bousmina M, Utracki LA. Polymer 2004;45:8403–13.
[37] Ray SS, Bousmina M. Macromol Rapid Commun 2005;26:450–5.
[38] Lee MW, Hu X, Yue CY, Li L, Tam KC. Compos Sci Technol 2003;63: 339–46.
[39] Lee MW, Hu X, Li L, Yue CY, Tam KC. Polym Int 2003;52:276–84.
[40] Zhang B, Ding Y, Chen P, Liu C, Zhang J, He J, et al. Polymer 2005;46: 5385–95.
[41] Wu L, Chen P, Zhang J, He J. Polymer 2006;47:448–56.
[42] White SA, Baird DG. J Non-Newtonian Fluid Mech 1986;20:93–101.
[43] White JL, Kondo A. J Non-Newtonian Fluid Mech 1977/1978;3: 41–64.
[44] Boger DV. Annu Rev Fluid Mech 1987;19:157–82.
[45] White JL. Appl Polym Symp 1973;20:155–74.
[46] Huneault MA, Shi ZH, Utracki LA. Polym Eng Sci 1995;35:115–27.
[47] Song CH, Isayev AI. Polymer 2001;42:2611–9.
[48] Bastida S, Eguiazabal JI, Nazabal J. Polymer 2001;42:1157–65.
[49] Wang H, Lee KW, Chung TS, Jaffe M. Polym Compos 2002;21:114–23.
[50] Saengsuwan S, Bualek-Limcharoen S, Mitchell GR, Olley RH. Polymer 2003;44:3407–15.
[51] Qin Y, Brydon DL, Mather RR, Wardman RH. Polymer 1993;34: 1196–201.
[52] Wang H, Tao X, Newton E, Chung TS. Polym J 2002;34:575–83.
[53] Lee MW, Hu X, Li L, Yue CY, Cheong LY. Compos Sci Technol 2003; 63:1921–9.
[54] Xu HS, Li ZM, Pan JL, Yang MB, Huang R. Macromol Mater Eng 2004; 289:1087–95.
[53] Machiels AGC, Denys KFJ, Van Dam J, De Boer AP. Polym Eng Sci 1996;36:2451–66.
[56] Serpe G, Jarrin J, Dawans F. Polym Eng Sci 1990;30:553–65.
[57] Kawaguchi M. Adv Colloid Interface Sci 1994;53:103–27.
[58] Raghavan SR, Riley MW, Fedkiw PS, Khan SA. Chem Mater 1998;10: 244–51.
[59] Liu CY, Zhang J, He JS, Hu GH. Polymer 2003;44:7529–32.
[60] Chiou BS, Raghavan SR, Khan SA. Macromolecules 2001;34:4526–33.
[61] Havet G, Isayev AI. Rheol Acta 2003;42:47–55.
[62] Shim SE, Isayev AI. Rheol Acta 2004;43:127–36.
[63] Yziquel F, Carreau PJ, Tanguy PA. Rheol Acta 1999;38:14–25.
[64] Wu G, Asai S, Sumita M, Hattori T, Higuchi R, Washiyama J. Colloid Polym Sci 2000;278:220–8.
[65] Krishnamoorti R, Giannelis EP. Macromolecules 1997;30:4097–102.
[66] Leblanc JL. Prog Polym Sci 2002;27:627–87.
[67] Krishnamoorti R, Yurekli K. Curr Opin Colloid Interface Sci 2001;6: 464–70.
[68] Cassagnau P. Polymer 2003;44:2455–62.
[69] Li J, Zhou CX, Wang G. J Appl Polym Sci 2003;89:3609–17.
[70] Yu W, Wu ZG, Zhou CX. Chem J Chin Univ 2003;24:715–8.
[71] Cogswell FN. Polym Eng Sci 1972;12:64–73.
[72] Cogswell FN. J Non-Newtonian Fluid Mech 1978;4:23–38.
[73] Muller AJ, Balsamo V, Silva FD, Rosales CM, Saez AE. Polym Eng Sci 1994;34:1455–63.
[74] Binding DM. J Non-Newtonian Fluid Mech 1988;27:173–89.
[75] He J, Bu W. Polymer 1994;35:5061–6.
[76] Yu W, Bousmina M, Zhou CX, Tucker CL. J Rheol 2004;48:417–38.